Nanotubular SnO_2 Templated by Cellulose Fibers: Synthesis and Gas Sensing

J. Huang,[†,‡] N. Matsunaga,[§] K. Shimanoe,[||] N. Yamazoe,[||] and T. Kunitake*[,†]

Topochemical Design Laboratory, Frontier Research System, The Institute of Physical and Chemical Research (RIKEN), Wako, Saitama 351-0198, Kitakyushu Foundation of the Advancement of Industry, Science and Technology, Hibikino, Wakamatsu, Kitakyushu, Fukuoka 808-0135, and Department of Molecular and Material Science, Interdisciplinary Graduate School of Engineering Sciences, Kyushu University, Kasuga-shi, Fukuoka 816-8580, Japan

Received December 14, 2004. Revised Manuscript Received April 4, 2005

SnO_2 nanotubular materials were prepared by using a natural cellulosic substance (filter paper) as template, and their morphologies were determined by scanning electron microscopy (SEM) and transmission electron microscopy (TEM). Cellulose fibers were first coated with SnO_2 gel layers by the surface sol−gel process using $Sn(O^iPr)_4$ as precursor, followed by calcination in air to give SnO_2 nanotubular materials as hollow replicas of natural cellulose fibers. The nanotubes obtained by calcination at 450 °C were amorphous-like and composed of fine particles with sizes smaller than ca. 5 nm. The outer diameters are tens to two hundred nanometers, and wall thicknesses are 10−15 nm. Calcination at 1100 °C yielded tubelike polycrystalline SnO_2 nanocages (outer diameter 100−200 nm), which were composed of rutile-phase SnO_2 nanocrystallites with sizes of 10−20 nm. The thermal behavior and the crystalline property of the powder obtained from calcination of the as-prepared SnO_2 sheet were examined in the temperature range of 300−900 °C. The sizes of the nanoparticle obtained by calcination at 300 and 900 °C were 2.0 and 9.2 nm, respectively, in fair agreement with TEM observation. Calcination temperatures above 500 °C are needed to obtain pure SnO_2. A sensor setup was fabricated from the SnO_2 nanotube sheet, and the sensor performance was measured for H_2, CO, and ethylene oxide. The sensor signal, *S*, was 16.5 at 450 °C to 100 ppm H_2, and was comparable to that of the conventional SnO_2 sensor. Finally, the sensor characteristics were discussed in relation to the morphology of the nanotube sheet.

Introduction

Being a stable wide-band-gap n-type semiconductor, SnO_2 is a promising key functional material for a wide range of practical applications. In particular, as a gas sensor is one of its well-known applications. The available sensors are generally made of tin oxide films or porous pellets. The importance of the utility factor in gas sensing by the oxide used (particle size, pore size, surface area, etc.) has been pointed out from the theoretical analysis.[1−3] Therefore, there is a newly emerging interest in one-dimensional nanostructured SnO_2 materials such as nanobelts, nanoribbons, and nanowires, apart from extensively studied SnO_2 films and nanoparticles. Recently, use of tin oxide nanobelts and nanowires to fabricate sensors for various gases such as carbon monoxide,[4−6] nitrogen dioxide,[5,7] and ethanol vapor[4,5] has been attempted.

Ribbonlike single-crystalline SnO_2 nanobelts were prepared by direct thermal evaporation[8−10] and laser ablation[11] of commercial SnO and SnO_2 powders through a vapor−solid (VS) process,[12] or by rapid oxidation of elemental tin,[13] both at high temperatures around 1000 °C. The well-established vapor−liquid−solid (VLS) process,[14−18] a tech-

* To whom correspondence should be addressed. Phone: +81-48-467-9601. Fax: +81-48-464-6391. E-mail: kunitake@ruby.ocn.ne.jp.

[†] RIKEN.

[‡] Present address: National Institute for Materials Science, Tsukuba, Ibaraki 305-0044, Japan.

[§] Kitakyushu Foundation of the Advancement of Industry, Science and Technology.

[||] Kyushu University.

(1) Yamazoe, N.; Sakai, G.; Matsunaga,; Baik, N. S.; Shimanoe, K. *Ceram. Trans.* **2002**, *130*, 27−36.
(2) Sakai, G.; Matsunaga, N.; Shimanoe, K.; Yamazoe, N. *Sens. Actuators, B* **2001**, *80*, 125−131.
(3) Matsunaga, N.; Sakai, G.; Shimanoe, K.; Yamazoe, N. *Sens. Actuators, B* **2002**, *83*, 216−221.
(4) Wang, Y.; Jiang, X.; Xia, Y. *J. Am. Chem. Soc.* **2003**, *125*, 16176−16177.
(5) Comini, E.; Faglia, G.; Sberveglieri, G.; Pan, Z.; Wang, Z. L. *Appl. Phys. Lett.* **2002**, *81*, 1869−1871.
(6) Kolmakov, A.; Zhang, Y.; Cheng, G.; Moskovits, M. *Adv. Mater.* **2003**, *15*, 997−1000.
(7) Law, M.; Kind, H.; Messer, B.; Kim, F.; Yang, P. *Angew. Chem., Int. Ed.* **2002**, *41*, 2405−2408.
(8) Pan, Z. W.; Dai, Z. R.; Wang, Z. L. *Science* **2001**, *291*, 1947−1949.
(9) Dai, Z. R.; Pan, Z. W.; Wang, Z. L. *Solid State Commun.* **2001**, *118*, 351−354.
(10) Dai. Z. R.; Gole, J. L.; Stout, J. D.; Wang, Z. L. *J. Phys. Chem. B* **2002**, *106*, 1274−1279.
(11) Hu, J.; Bando, Y.; Liu, Q.; Golberg, D. *Adv. Funct. Mater.* **2003**, *13*, 493−496.
(12) Brenner, S. S.; Sears, G. W. *Acta Metall.* **1956**, *4*, 268−270.
(13) Hu. J. Q.; Ma, X. L.; Shang, N. G.; Xie, Z. Y.; Wong, N. B.; Lee, C. S.; Lee, S. T. *J. Phys. Chem. B* **2002**, *106*, 3823−3826.
(14) Wagner, R. S.; Ellis, W. C. *Appl. Phys. Lett.* **1964**, *4*, 89−90.
(15) Morales, A. M.; Lieber, C. M. *Science* **1998**, *279*, 208−211.
(16) Duan, X.; Lieber, C. M. *Adv. Mater.* **2000**, *12*, 298−302.
(17) Duan. X.; Huang, Y.; Cui, Y.; Wang, J.; Lieber, C. M. *Nature* **2001**, *409*, 66−69.

10.1021/cm047819m CCC: $30.25
Published on Web 06/04/2005

nique for catalyst-guided nanowire growth via thermal evaporation, was employed to synthesize nanowires of SnO_2[19,20] or indium-doped SnO_2[21] at intermediate temperatures. In the VLS process, a liquid metal droplet acts as the catalytic active site for absorption of gas-phase reactants and leads to nanowire growth. The catalyst determines the wire size, and the resultant nanowire has a solid catalyst nanoparticle at the tip. The nanostructured SnO_2 materials produced by the above-mentioned thermal evaporation methods are usually of low purity, and they are frequently composed of mixtures of several different morphologies. A reverse microemulsion-mediated solvothermal process (conducted at 200 °C) was recently developed as low-temperature synthesis to fabricate crystalline SnO_2 nanorods.[22] But the aspect ratio of the synthesized nanorod is rather low. Another newly reported solution method provides polycrystalline SnO_2 nanowires, which are composed of interconnected rutile-phase nanocrystallites.[4]

In contrast to these methods that produce solid wirelike nanostructured SnO_2, reports on hollow nanotubular SnO_2 materials are quite rare. SnO_2 nanotubes possess higher surface-to-volume ratios, as a key feature in practical applications such as catalysts and gas sensing. The SnO_2 nanotube obtained by high-temperature synthesis is rather nonuniform, and the hollow core is not continuous through the length of the sample.[10] A recent vapor deposition process based on the VLS growth mechanism gives single-crystal nano- and microtubes of SnO_2 with rectangular cross-sections and sealed ends on quartz substrates.[23]

In the present work, we demonstrate an efficient, facile approach for synthesis of SnO_2 nanotubular materials in large quantities. It is based on the surface sol−gel process[24−27] as applied to covering of cellulose fibers (filter paper) with a SnO_2 gel layer with nanometer precision. Subsequent calcination of the as-prepared SnO_2 gel/filter paper composite (as-prepared SnO_2 sheet) resulted in SnO_2 nanotubes. This approach is useful for developing nanoprecision oxide materials and provides an effective means to examine the influence of morphology (utility factor) on sensor properties.

Experimental Section

Preparation of SnO_2 Nanotube Sheets. Tetraisopropoxytin−2-propanol adduct, ($Sn(O^iPr)_4 \cdot {}^iPrOH$, Gelest) was used as received. 2-Propanol and methanol were guaranteed reagents and used without further purification. Water used was purified using a Milli-Q system from Millipore. Filter paper (quantitative ashless) was purchased from Advantec Toyo (Tokyo, Japan).

Surface sol−gel deposition of SnO_2 gel layers was carried out at about 50 °C. In a typical deposition procedure, a piece of filter paper was placed in a suction filter funnel, and was washed by suction filtration of ethanol, followed by drying with air flow. Ten milliliters of $Sn(O^iPr)_4 \cdot {}^iPrOH$ in 1:1 (v/v) 2-propanol/methanol (10 mM) was then added to the filter funnel. The first 5 mL of the solution was slowly suction-filtered through the filter paper, and the rest was left to stand for 3 min to ensure adsorption of tin alkoxide. The remaining 5 mL of solution was thereafter suction-filtered slowly through the filter paper, and immediately two 20 mL portions of 2-propanol/methanol (1:1, v/v) were filtered to remove the excessively adsorbed, unreacted tin alkoxide. Twenty milliliters of water was then added to the funnel and allowed to pass through the filter paper slowly within 3 min to promote hydrolysis of tin alkoxide and condensation of the resultant SnO_2 gel layer. The filter paper was finally dried with air flow to finish the deposition cycle. Individual cellulose fibers in the filter paper were thus coated with a nanometer-thick SnO_2 gel layer. The deposition cycle was repeated a given number of times. The as-prepared SnO_2 gel/filter paper composite was subjected to calcination in air at 450 °C (heating rate 1 °C/min) or at 1100 °C (heating rate 3 °C/min) for 6 h to remove the original filter paper. In both cases, white sheets composed of SnO_2 nanotubes were obtained.

Characterization. The obtained white sheet of SnO_2 was first observed by field emission scanning electron microscopy (FE-SEM) and transmission electron microscopy (TEM). Specimens were prepared as follows: the white sheet product was sonicated in ethanol for about 20 s to dispense as a suspension. A drop of the suspension was placed on a silicon wafer (for FE-SEM observation) or on a silicon oxide-coated gold grid (for TEM observation) and allowed to dry in air. FE-SEM measurements were conducted using a Hitachi S-5200 microscope operated at an acceleration voltage of 25.0 kV, and TEM observations were carried out with a JEOL JEM-2000 instrument working at 120 kV accelerating voltage.

The thermogravimetric analysis (TGA; TG8120IRA, Rigaku, Japan) of the as-prepared SnO_2 sheet was carried out to trace the calcination process. The as-prepared SnO_2 sheet was milled and subjected to analysis at a heating rate of 10 °C/min from room temperature to 1300 °C with air flow at 100 cm^3/min. The crystal morphology of the resulting SnO_2 nanotube product was examined by X-ray diffraction (XRD; XRD-DSC-X II, Rigaku, Japan). A piece of the as-prepared SnO_2 sheet was milled, and the resulting powder was heated at a rate of 3 °C/min to 300 °C and calcined at this temperature for 3 h. The XRD pattern of the resulting SnO_2 was recorded from $2\theta = 20°$ to $2\theta = 80°$ at room temperature. XRD patterns were measured after similar treatment every 100 °C up to 900 °C. The size of the resulting SnO_2 crystallites was evaluated from diffraction peaks of (110), (101), and (211) by using Scherrer's equation, and their mean value was adopted as an average crystallite size (*D*, diameter).

Measurement of Gas-Sensing Properties. A piece of as-prepared SnO_2 sheet was cut into quadrilateral sheets of about 2 × 4 mm and fixed with gold paste onto an alumina substrate attached with gold electrodes having a gap of 1 mm. The whole assembly was calcined at 500 °C for 3 h in air. Gas-sensing experiments were carried out as reported,[28] in a gas flow apparatus equipped with an external heating facility in the temperature range of 350−500 °C. The sample gas used was 100 ppm H_2, 100 ppm CO, or 20 ppm ethylene oxide (C_2H_4O), diluted in dry air. The gas flow

(18) Ding, Y.; Gao, P. X.; Wang, Z. L. *J. Am. Chem. Soc.* **2004**, *126*, 2066−2072.
(19) Chen, Y.; Cui, X.; Zhang, K.; Pan, D.; Zhang, S.; Wang, B.; Hou, J. G. *Chem. Phys. Lett.* **2003**, *369*, 16−20.
(20) Liu, Z.; Zhang, D.; Han, S.; Li, C.; Tang, T.; Jin, W.; Liu, X.; Lei, B.; Zhou, C. *Adv. Mater.* **2003**, *15*, 1754−1757.
(21) Nguyen, P.; Ng, H. T.; Kong, J.; Cassell, A. M.; Quinn, R.; Li, J.; Han, J.; McNeil, M.; Meyyappan, M. *Nano Lett.* **2003**, *3*, 925−928.
(22) Zhang, D.-F.; Sun, L.-D.; Yin, J.-L.; Yan, C.-H. *Adv. Mater.* **2003**, *15*, 1022−1025.
(23) Liu, Y.; Dong, J.; Liu, M. *Adv. Mater.* **2004**, *16*, 353−356.
(24) Ichinose, I.; Senzu, H.; Kunitake, T. *Chem. Lett.* **1996**, 831−832.
(25) Ichinose, I.; Senzu, H.; Kunitake, T. *Chem. Mater.* **1997**, *9*, 1296−1298.
(26) Ichinose, I.; Lee, S.-W.; Kunitake, T. In *Supramolecular Organization and Materials Design*; Jones, W., Rao, C. N. R., Eds.; Cambridge University Press: Cambridge, U.K., 2002; pp 172−213.
(27) Huang, J.; Ichinose, I.; Kunitake, T.; Nakao, A. *Langmuir* **2002**, *18*, 9048−9053.
(28) Baik, N. S.; Sakai, G.; Miura, N.; Yamazoe, N. *Sens. Actuators, B* **2000**, *63*, 74−79.

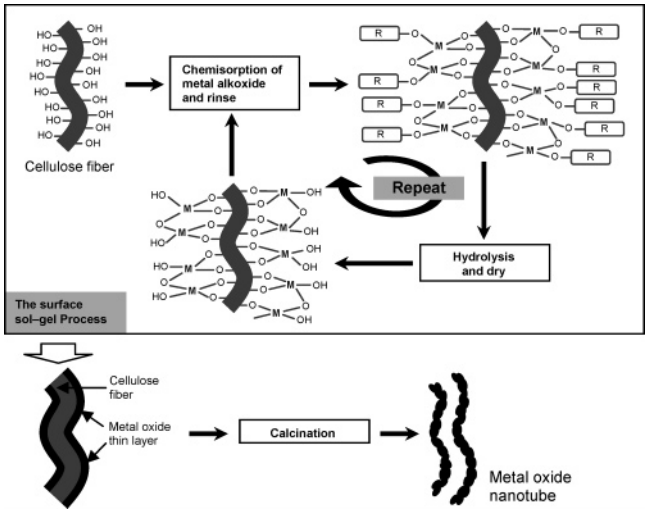

Figure 1. Representative illustration of metal oxide nanotube synthesis by applying the surface sol−gel process on cellulose fibers.

(100 cm^3/min) was switched between the sample gas and dry air while the electrical resistance of the SnO_2 nanotube sheet was measured continuously on an electrometer. The sensor signal, S, is defined as the resistance ratio, R_a/R_g, where R_a and R_g stand for the electrical resistance in dry air and in the sample gas, respectively.

Results and Discussion

Fabrication of SnO_2 Nanotube Sheets. We have demonstrated that the surface sol−gel process is a facile chemical method to deposit ultrathin metal oxide layers with molecular precision.[24−26] As illustrated in Figure 1, this process is based on chemical adsorption of metal alkoxide from solution onto a hydroxylated substrate surface to form a covalently bound monolayer, followed by hydrolysis to give a new hydroxylated gel layer for successive film deposition. Subnanometer thickness can be attained for an individual metal oxide layer under carefully controlled experimental conditions.[27] Organic molecules can be readily incorporated as second components if they are reactive with the as-deposited amorphous metal oxide layer,[26,29] and their sizes and shapes can be accurately traced by the metal oxide network.[30,31]

Natural cellulose fibers possess abundant surface hydroxyl groups, and provide a suitable substrate for metal oxide deposition via the surface sol−gel process. We have recently developed an "artificial fossil approach" to obtain metal oxide nanotubes by using natural cellulose materials such as filter paper, cloth, and cotton as templates.[32] Applying the conventional sol−gel process on the cellulose acetate template could not produce metal oxide nanotubes; only porous metal oxide was obtained.[33] In the artificial fossil approach, ultrathin metal oxide gel films are deposited on morphologically complex surfaces of the cellulosic substances with nanometer precision. Their hierarchical morphologies are retained in metal oxide films to give macroscopic fossils after removal of the organic substances by calcination. A similar approach was employed to prepare SnO_2 nanotubular materials from filter paper. SnO_2 gel layers are deposited to coat the individual cellulose fibers by repeating the surface sol−gel deposition cycle. Figure 2 shows morphologies of SnO_2 nanotubes yielded by calcination of an as-prepared SnO_2 sheet at 450 °C. The surface sol−gel deposition was repeated 12 times for this sample. As displayed in the inset of Figure 2a, the calcined self-supporting SnO_2 sheet possesses overall morphological characteristics of the initial filter paper except for a little shrinkage in size. The SnO_2 sheet is composed of irregular nanotube assemblies, as shown by this overview FE-SEM image. Individual nanotubes can be clearly distinguished in a higher magnification SEM micrograph (Figure 2b). The outer diameters of the nanotube range from a few tens of nanometers to ca. two hundred nanometers. Being replicas of the natural cellulose fiber, the SnO_2 nanotubes possess very high aspect ratios. The Figure 2b inset shows the broken surface and the hollow morphology of a nanotube. The thickness of the tube wall is estimated to be 10−15 nm from the broken surface. Since the surface sol−gel deposition was repeated for 12 cycles, 1-cycle deposition corresponds to ca. 1 nm wall thickness. This is close to the titania case.[32a] The tubular morphology was also characterized by TEM, as revealed in Figure 2c. The hollow cagelike tube structure is clearly identified, and the wall thickness (10−15 nm) is seen to be uniform along its entire length. The SnO_2 nanotubes are composed of fine particles with sizes smaller than ca. 5 nm (Figure 2d), and the fine particle (calcined at 450 °C) is most likely in an amorphous state and may contain certain impurities because no typical crystalline structure was observed in the electron diffraction measurement of the nanotube assembly.

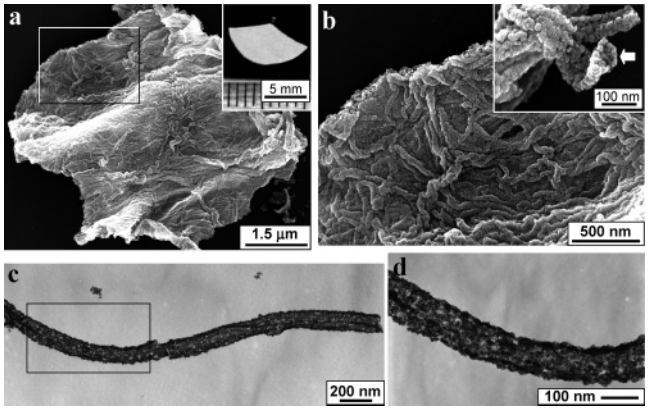

Figure 2. SnO_2 nanotubes yielded by calcination of a SnO_2 gel/filter paper composite sheet at 450 °C. (a) Low-magnification field emission scanning electron micrograph of the SnO_2 nanotube sheet, showing nanotube assemblies. The inset is a macroscopic photograph of the sheet, which was obtained by calcination of one-third of an as-prepared sheet. (b) FE-SEM image of the morphological details of the boxed area in (a). The inset shows the high-magnification FE-SEM image of two individual SnO_2 nanotubes; the arrow indicates an opening of the nanotube. (c) Transmission electron micrograph of one individual SnO_2 nanotube isolated from the assembly. (d) High-magnification TEM image of the boxed area in (c).

In previous examples given by other research groups, cotton fibers were employed as a template for the preparation

(29) Ichinose, I.; Kawakami, T.; Kunitake, T. *Adv. Mater.* **1998**, *10*, 535−539.
(30) Huang, J.; Ichinose, I.; Kunitake, T. *Chem. Commun.* **2002**, 2070−2071.
(31) For a recent review, see: Kunitake, T.; Lee, S.-W. *Anal. Chim. Acta* **2004**, *504*, 1−6.
(32) (a) Huang, J.; Kunitake, T. *J. Am. Chem. Soc.* **2003**, *125*, 11834−11835. (b) Caruso, R. A. *Angew. Chem., Int. Ed.* **2004**, *43*, 2746−2748.
(33) Caruso, R. A.; Schattka, J. H. *Adv. Mater.* **2000**, *12*, 1921−1923.

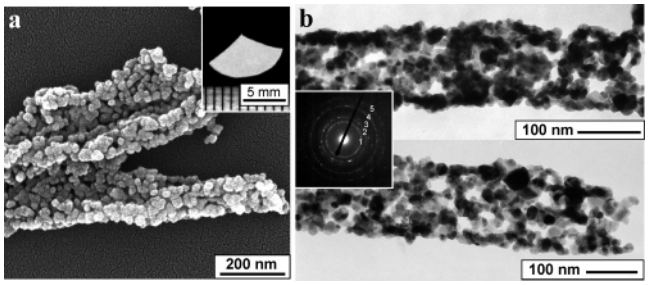

Figure 3. SnO_2 nanotubes obtained by calcination of a SnO_2 gel/filter paper composite sheet at 1100 °C. (a) FE-SEM image of the SnO_2 nanotube assembly. The inset shows a macroscopic photograph of the nanotube sheet, which was obtained by calcination of one-third of an as-prepared sheet. (b) TEM images of individual SnO_2 nanotubes isolated from the assembly. The inset is the selected-area electron diffraction (SAED) pattern from the nanotube assembly.

of SnO_2 microtubes by the chemical deposition technique through olation and heterogeneous nucleation of tin difluoride.[34] The initial template morphology was replicated only on the micrometer scale by the SnO_2 matrix, resulting in SnO_2 tubules with diameters and wall thicknesses in the micrometer regime. Only by taking advantage of the surface sol−gel process, the natural cellulosic substance can be replicated at all levels of morphological hierarchies from nanometer to centimeter regimes.

When an as-prepared SnO_2 sheet was calcined at 1100 °C, a similar self-supporting ceramic sheet was obtained as a macroscopic fossil of the template filter paper, as shown in the Figure 3a inset (deposition of SnO_2 gel thin films was repeated 12 times for this sample). As shown by the electron micrographs displayed in Figure 3, the resulting SnO_2 possesses a tubelike nanocage morphology with a hollow tube wall. This tubular nanocage is apparently composed of a network of interconnected SnO_2 particles with sizes of 10−20 nm, and the outer diameter of the nanocage varies from ca. 100 to ca. 200 nm. Its selected-area electron diffraction (SAED) pattern (Figure 3b inset) reveals that the nanoparticle is crystalline with the tetragonal rutile structure (cassiterite), and diffraction rings 1−5 are indexed to (110), (101), (200), (210), and (211) diffraction of rutile-phase SnO_2, respectively. All the diffractions are constituted by continuous rings and individual spots. This indicates that the nanocage is composed of fine crystal particles with partial orientation. Thus, the as-deposited SnO_2 gel layer is converted into cassiterite nanocrystallites through high-temperature (1100 °C) calcination, while maintaining the nanofibrous morphology of the initial filter paper.

Additional Structural Analysis. The conditions of thermal treatment strongly affect the structure and sensor property of the SnO_2 nanotubes formed. Therefore, we conducted a more careful examination of the SnO_2 phase change with thermal treatment. Figure 4 shows TGA and its differential curves for an as-prepared SnO_2 sheet. As seen from the differential curve, the sample experienced two-step weight losses at 71 and 319 °C. These peaks represent evaporation of solvents (2-propanol and methanol) and combustion of the organic moiety, respectively. The weight

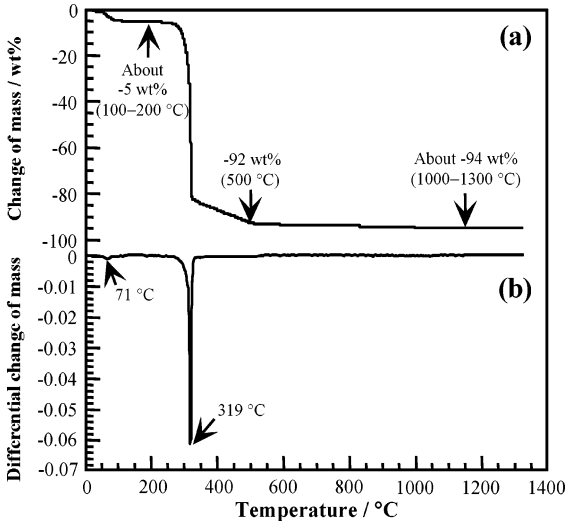

Figure 4. (a) Thermogravimetric analysis and its differential curve (b) for an as-prepared SnO_2 sheet.

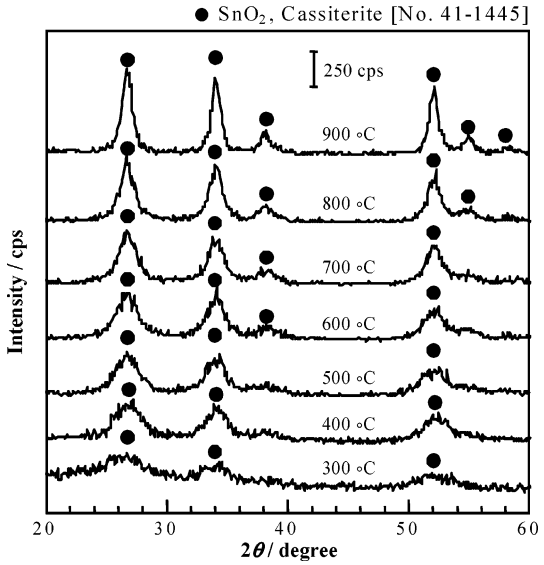

Figure 5. XRD patterns of the SnO_2 powder obtained by calcination of the as-prepared SnO_2 sheet for 3 h at various temperatures.

loss was 92 wt % up to 500 °C and then slightly decreased to reach 94 wt % at 1300 °C. It is clear that calcination temperatures above 500 °C are needed to obtain pure SnO_2 from the as-prepared composite sheet. Figure 5 shows XRD patterns of such SnO_2 powders obtained at different calcination temperatures from 300 to 900 °C. All diffraction peaks agree with the tetragonal structure (rutile type) in JCPDS 41-1445 (cassiterite), which indicates that the specimens consist of SnO_2. The intensity of each peak increased with increasing calcination temperature. In particular, the sample calcined at a temperature above 500 °C showed typical diffraction peaks of cassiterite, suggesting that the sample is composed of pure SnO_2 without any indication of other crystalline impurities. Figure 6 shows the crystallite size (D) as a function of calcination temperature. D is determined from the full width of half-maximum (fwhm) and Bragg angle, as described in the Experimental Section. D is seen to increase gradually up to 700 °C, but more quickly after that temperature. Interestingly, the D value of the powder calcined at 300 °C was only about 2.0 nm. This is smaller

(34) Imai, H.; Iwaya, Y.; Shimizu, K.; Hirashima, H. *Chem. Lett.* **2000**, 906−907.

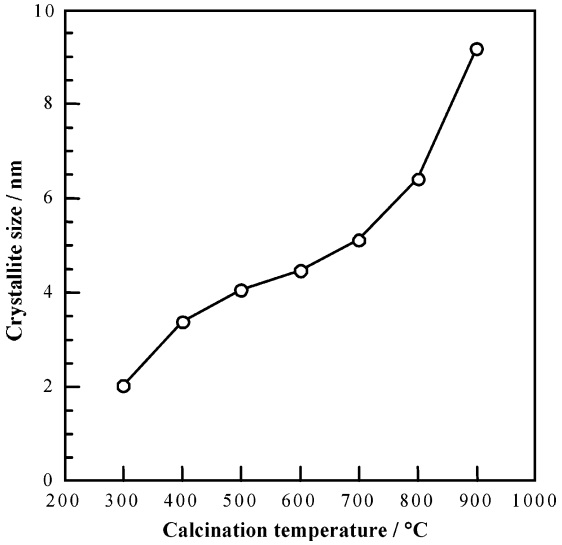

Figure 6. Dependence of SnO_2 crystallite size on calcination temperatures.

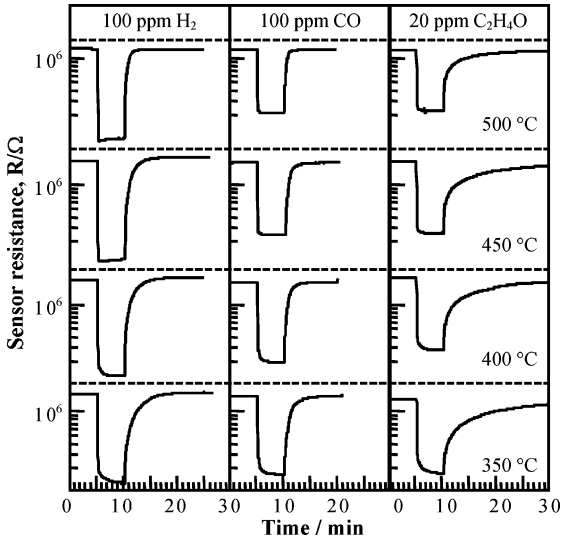

Figure 7. Response transients of SnO_2 nanotubes to 100 ppm H_2, 100 ppm CO, and 20 ppm C_2H_4O at various temperatures.

than that of SnO_2 derived from $SnCl_4$ (about 4 nm at 300 °C).[35] Even at the calcination temperature of 900 °C, *D* was suppressed to below 10 nm. TEM observation in Figures 1 and 2 indicates that the sizes of SnO_2 nanoparticles are ca. 5 and 10−20 nm at calcination temperatures of 450 and 1100 °C, respectively. These data are in fair agreement with crystallite sizes estimated for each calcination temperature, although the two sets of data for 1100 °C cannot be directly compared. In any case, it is clear that crystal growth is suppressed even at high calcination temperatures. Such suppressed crystal growth of SnO_2 has been reported in the past, only for that of hydrothermally treated SnO_2 derived from $SnCl_4$[36] or from Na_2SnO_3.[37] The mechanism of the suppression effect in our case is not clear. It may arise from the unique preparation process of the SnO_2 sheet. SnO_2 nanoparticles are formed separately on the cellulose fiber matrix and probably possess limited numbers of contacts with the neighboring particles in the sheet. But the details need to be worked out in future research.

Sensor Property. The unique nanocage morphology of the SnO_2 nanotubes could offer advantages in fabricating gas sensors. The high surface area and the fine grain size could enhance the interaction between SnO_2 surface and gas molecules to be detected, and the nanocage structure would facilitate fast and full gas access to SnO_2 nanocrystals. In the case of a conventional thin-film SnO_2 sensor, concentration gradients of sensing gases may arise between the outermost layer of the film and the bottom layer directly attached to the electrode substrate. Open nanotubes will not have this problem. The tubular SnO_2 nanocages are hence expected to provide better gas sensitivity and sensing reversibility compared with SnO_2 films or nanobelts.

Figure 7 shows response transients of a SnO_2 nanotube sheet sensor to 100 ppm H_2, 100 ppm CO, and 20 ppm

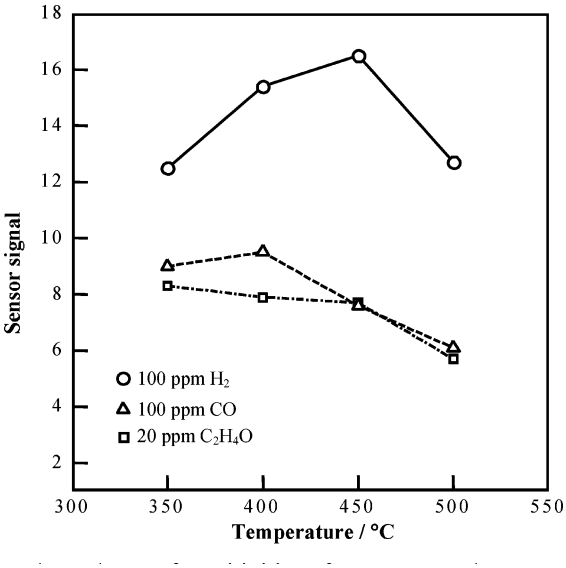

Figure 8. Temperature dependence of the sensitivities of the SnO_2 nanotube sensor to 100 ppm H_2, 100 ppm CO, and 20 ppm C_2H_4O.

ethylene oxide in the working temperature range of 350−500 °C. The resistance (R_a) of the sensor in dry air was (1−2) × 10^6 Ω at the tested temperatures and increased slightly with decreasing temperature. This R_a level is close to that of the SnO_2 crystallite.[28] Among the gases tested, the response transient to the smallest hydrogen gas was larger than those to the other two gases, although a low concentration range was employed for ethylene oxide. According to previous reports,[2,3] the sensitivity to the target gas strongly depends on the ease of diffusion of gas molecules inside the sensor. It is clear that the hydrogen molecule is diffused most easily inside the deeper region of the sensor and reacts with oxygen adsorbed on the SnO_2 surface. Figure 8 shows the dependence of the sensor signal, *S*, of the test gases on the working temperature. The sensor signal to hydrogen gas gives a concave shape with a peak at 450 °C, while *S* values to the other two gases show downward trends with temperature. Unfortunately, these *S* values at 450 °C seem not to be so high, compared with other reported results (*S* values are 500 and 1150 to 800 ppm H_2 and 800 ppm CO, respectively, at

(35) Xu, C.; Tamaki, J.; Miura, N.; Yamazoe, N. *Sens. Actuators, B* **1991**, *3*, 147−155.
(36) Baik, N. S.; Sakai, G.; Miura, N.; Yamazoe, N. *J. Am. Ceram. Soc.* **2000**, *83*, 12, 2983−2987.
(37) Matsunaga, N.; Sakai, G.; Shimanoe, K.; Yamazoe, N. *Abstr. 9th Int. Meet. Chem. Sens.* **2002**, 138.

350 °C).[28] The grain size effect is well-known for the SnO_2 gas sensor, and the gas sensitivity increases drastically with crystallite size (D) of less than 6 nm.[35] The known relationship of D and sensitivity predicts that the gas sensor signal of the current SnO_2 nanotube could be much larger than the observed value. The present SnO_2 sheet is rather thick (ca. 0.2 mm) and is composed of highly entangled nanotubes. Therefore, the access of gas molecules to SnO_2 nanotubes may not be favored, compared with that toward isolated nanotubes and to bundles of a few nanotubes, or general SnO_2 nanocrystalline films[38,39] and nanowires/belts.[4−7] It is also essential that either nanotubes have a porous wall or the tube ends are open, to secure efficient access of gaseous reactants. Such favorable situations are apparently not attained in our case, and the sensitivity is not superior to that of the thin-film SnO_2 sensors.

Conclusions

Natural cellulosic substances such as filter paper act as superior templates to synthesize SnO_2 nanotubular materials by combination of the surface sol−gel process and subsequent calcination. The resulting nanotube sheet retains the morphological hierarchy of the filter paper, and each nanotube is composed of SnO_2 nanocrystals of a few nanometers. Its sensitivity as sensor to H_2 and other gases was not as good as expected from its extremely large surface area. This may be attributed to insufficient access of the test gases to SnO_2 nanocrystals due to its morphology. It appears that the sensor capability of individual SnO_2 nanotubes is not expressed in our case. Isolated and/or better aligned nanotubes could lead to enhanced gas access. Our efforts will be directed to fabrication of aligned bundles of SnO_2 nanotubes.

CM047819M

(38) Graf, M.; Barrettino, D.; Taschini, S.; Hagleitner, C.; Hierlemann, A.; Baltes, H. *Anal. Chem.* **2004**, *76*, 4437−4445.

(39) Pinna, N.; Neri, G.; Antonietti, M.; Niederberger, M. *Angew. Chem., Int. Ed.* **2004**, *43*, 4345−4349.